Enhanced electrochemical reduction of hydrogen peroxide by Co_3O_4 nanowire electrode

Wonwoo Jeong[a], Cui-Lei Yin[b], Kwan San Hui[c*], Kwun Nam Hui[d*], Young Rae Cho[a], Kyung Mox Cho[a*]

[a]School of Materials Science and Engineering, Pusan National University, San 30 Jangjeon-dong, Geumjeong-gu, Busan 609-735, Republic of Korea

[b]Department of Manufacturing Engineering and Engineering Management, City University of Hong Kong, Kowloon Tong, Hong Kong

[c]School of Mathematics, University of East Anglia, Norwich, NR4 7TJ, United Kingdom

[d]Institute of Applied Physics and Materials Engineering, University of Macau, Avenida da Universidade, Macau, China

*Corresponding author:

E-mail: k.hui@uea.ac.uk (Kwan San Hui)

E-mail: bizhui@umac.mo (Kwun Nam Hui)

E-mail: chokm@pusan.ac.kr (Kyung Mox Cho)

Abstract

Crystalline Co_3O_4 nanowire arrays with different morphologies grown on Ni foam were investigated by varying the reaction temperature, the concentration of precursors, and reaction time. The Co_3O_4 nanowires synthesized under typical reaction condition had a diameter range of approximately 500–900 nm with a length of 17 μm. Electrochemical reduction of hydrogen peroxide (H_2O_2) of the optimized Co_3O_4 nanowire electrode was studied by cyclic voltammetry. A high current density of 101.8 mA cm^{-2} was obtained at -0.4 V in a solution of 0.4 M H_2O_2 and 3.0 M NaOH at room temperature compared to 85.8 mA cm^{-2} at -0.35 V of the Co_3O_4 nanoparticle electrode. Results clearly indicated that the Ni foam supported Co_3O_4 nanowire electrode exhibited superior catalytic activity and mass transport kinetics for H_2O_2 electrochemical reduction.

Keywords: Co_3O_4; Nanowire arrays; Ni form; H_2O_2 electrochemical reduction

1. Introduction

Recently, the development of hydrogen peroxide (H_2O_2) as an oxidant for low-temperature liquid-based fuel cells has attracted significant attention due to lower activation energy, better stability, and ease of handling and storage compared to oxygen based fuel cells [1-3]. Lao et al. has shown that electrochemical reduction of H_2O_2 has faster kinetics than that of oxygen [4]. Yin et al. has demonstrated a direct hydrazine/H_2O_2 fuel cell exhibiting an open circuit voltage (OCV) of ~1.6 V and a high power density of 470 mW cm^{-2} compared to that with oxygen oxidant (OCV~0.9 V and 73.9 mW cm^{-2}) [5]. To date, noble metals such as Pt, Pd, Ir, Au, and Ag are the dominant catalysts for electrochemical reduction H_2O_2 owing to the high efficiency and stability [6-9]. However, the expensive cost and scarcity of noble metal resources hinder their practical applications. Therefore, current research focuses on the electrochemical reduction of H_2O_2 using transitional metal oxides such as nickel oxide, iron oxide, copper oxide due to their low cost, high abundance, and high electrocatalytic reaction [10].

Among the transitional metal oxides, cobalt oxide (Co_3O_4) has been extensively studied because of its superior catalytic properties arise from its efficient electron transportation between Co^{2+} and Co^{3+} ions [11, 12]. However, Co_3O_4 catalysts usually suffer from the poor electrical conductivity and the dissolution or agglomeration during electrochemical processes [13]. Therefore, mixing Co_3O_4 catalysts with conductive carbon-based materials such as carbon nanotubes, graphene, and carbon foam is proposed to improve the conductivity of the Co_3O_4 hybrid catalysts [14]. However, such mixing approach involves the use of an organic binder, which will decrease the effective surface area of

the Co_3O_4 catalysts [15]. Accordingly, a binder-free approach by directly growing the electrocatalyst materials on a current collector such as carbon-based materials has proved to enhance the cycling stability of the electrocatalysts [16, 17]. Also, one-dimensional (1D) nanostructure have been reported to be a promising morphology for high electrochemical performance owing to their sufficient exposed surface, efficient ion transfer and rapid electron transport [18, 19].

In this work, various synthesis conditions including the influence of reaction temperature, the concentration of precursors, and reaction time on the morphology of 1D Co_3O_4 nanostructures grown on Ni foam were comprehensively investigated. The optimized Co_3O_4 nanowire electrode was selected to study the electrochemical reduction of H_2O_2 in alkaline medium. For comparison, the electrochemical reduction of H_2O_2 in conventional powdery Co_3O_4 nanoparticle electrode was studied. The Co_3O_4 nanowire electrode delivered a high current density of 101.8 mA cm^{-2} at -0.4 V in a solution of 0.4 M H_2O_2 and 3.0 M NaOH at room temperature compared to 85.8 mA cm^{-2} at -0.35 V of the Co_3O_4 nanoparticle electrode.

2. Experimental

2.1. Ni Foam Supported Co_3O_4 Nanowire Arrays

Ni foam substrate (110 PPI, 320 g m^{-2}; Artenano Company Limited, HK) was cleaned in acetone for 10 min, then etched with 6.0 M HCl for 30 min. After thoroughly rinsing with water, the Ni foam was soaked in 0.1 mM $NiCl_2$ for 8 h and extensively rinsed with water.

Various amount of $Co(NO_3)_2$ and NH_4NO_3 were added in a solution consisting of deionized water and ammonia (30 wt%). The homogeneous solution containing 0.2 M $Co(NO_3)_2$ and 0.1 M NH_4NO_3 was magnetically stirred for 20 min in air at room temperature until the pink color solution was gradually turned to black color. Such change of color indicates that Co(II) ions were partially oxidized to Co(III) ions in the solution through the uptake of oxygen. Ammonia added to the solution might enhance the oxidation of Co(II) ions to Co(III) ions [20]. The pretreated Ni foam and the obtained homogeneous solution were then transferred to a Teflon-lined stainless-steel autoclave, which was sealed and kept at different temperatures and maintained for different reaction times. To investigate the impact of various synthesis parameters on the morphology of the nanowire grown on the Ni foam, a series of conditions were tested and summarized in Table 1. After the reaction, the Ni foam with as-synthesized products was taken out from the solution and thoroughly washed with water, dried at 80 °C. Then, the Ni foam with as-grown Co_3O_4 precursors were calcined at 300º C for 2 h. Notably, the merging of Co_3O_4 nanowires occurred when the thermal treatment temperature was higher than 300º C [21]. For comparison, the morphology of the nanowire arrays was examined using scanning electron microscopy (SEM, JEOL JSM-5600) and transmission electron microscopy (TEM, FEI Teccai G2 S-Twin, Philips). The structure was determined using an X-ray diffractometer (XRD, Siemens D500). The 2θ scan range was from 10° to 80° with a scan rate of 5 ° min^{-1} and a step width of 0.02°.

2.2. H_2O_2 Electroreduction

Cyclic voltammetric tests were conducted on an IVIUM nSTAT electrochemical station. Ni foam supported binder-free Co_3O_4 nanowire electrode and powdery Co_3O_4 nanoparticle electrode were working electrodes. The powdery Co_3O_4 nanoparticle electrode was prepared by mixing the active material (5 mg), acetylene black, and polytetrafluorene-ethylene (PTFE) binder at a weight ratio of 80:15:5 and dispersing the mixture in ethanol to produce a homogeneous paste. The mixture was carefully placed onto nickel foam (1 cm × 1 cm × 0.2 cm), and then dried in a vacuum oven at 80 °C before pressing under a pressure of 20 MPa. A glassy carbon rod behind a D-porosity glass frit and a saturated Ag/AgCl, KCl electrode was employed as the counter and reference electrodes, respectively. All electrochemical tests were performed at room temperature. The electrolyte was a 3.0 M aqueous NaOH solution made using analytical grade chemical reagents.

3. Results and discussion

To study the effect of time on the morphology of the nanowire arrays grown on the Ni foam, different reaction times were tested ranging from 3 to 18 h (Table 1, Samples 1–4). Figure 1a-c shows the morphological and structural evolution of the nanowires grown on the Ni foam at different reaction times. The shiny Ni foam substrate turned black after nanowire growth. Both the size and uniformity of the nanowires increased with prolongation of reaction time. For the reaction time of 12 h (Sample 3), the Co_3O_4 nanowires were structurally uniform and had diameters of approximately 500–900 nm and lengths of up to 17 μm. However, when the reaction time reached 18 h, the nanowires

(Fig. 1d, Sample 4) became slightly lengthened, and the uniformity became degraded. A number of nanoparticles were deposited onto the surface of the nanowires. The reason might be that some high-energy sites were formed due to the effect of ammonia and vapor-liquid equilibrium, causing Co ions to nucleate spontaneously onto these active sites and to form nanoparticles. It was reported that hydrazine hydrate as a bidentate ligand can play a structure-directed role in the formation of β-$Co(OH)_2$ nanocolumns [22]. Ammonia is expected to play a similar role in the nanowire growth because ammonia is a unidentate ligand and it can form complexes with Co(II) ions and Co(III) ions.

The proposed evolution process is as follows. At the early stage of the reaction, the adsorption of Co(II) cations on the Ni foam increased the local cation concentration and formed the nuclei. The dominant β-$Co(OH)_2$ nanowires were then formed from the nuclei during the initial 6 h reaction [23, 24] (Samples 1–2). When the reaction time was prolonged to 12 h, the surface of nanowire became granular. A clear Co_3O_4 spinel phase was identified, as supported by the XRD pattern (Fig. 4a). The granular morphology of the Co_3O_4 nanowires was due to the solid-state reaction between the β-$Co(OH)_2$ nanowires and the dissolved oxygen in the solution. These results, combined with the XRD results (Fig. 4a), confirm that the as-prepared nanowires consisted of brucite β-$Co(OH)_2$ and spinel Co_3O_4 phases, which suggest the partial oxidation of Co(II) ions to Co(III) ions during the nanowire growth [21]. The oxidation reaction from β-$Co(OH)_2$ to Co_3O_4 was considered as energetically favored transformation [25]. Notably, the β-$Co(OH)_2$ nanowire was transformed to Co_3O_4 nanowire without a significant increase in diameter. Figure 2 shows the Co_3O_4 samples synthesized under different concentrations

of precursors (Samples 5–8). The results suggest that low reactant concentration of the reactant (Sample 5) could not sustain the growth of nanowires but only caused the formation of compact and non-uniform nanoplates on the surface of the Ni foam. The mechanism of nanoplate growth was complicated and influenced by various factors. The dominant phase of the as-prepared nanocrystal produced in the initial stage of reaction (non-calcined) was the brucite β-$Co(OH)_2$ phase, which had a layered structure and comprised sheets of hexagonally close-packed OH ions with one Co(II) ions bonded to six OH ions. These β-$Co(OH)_2$ sheets were bonded to one another by weak OH-OH dipole interactions. Therefore, brucite crystals have the tendency to grow into thin nanoplates. When the concentration of reactants was low (Sample 5), the amount of reactant could not sustain the growth of nanowires. Thus, a compact thin film of β-$Co(OH)_2$ nanoplates were produced. After calcination in air, β-$Co(OH)_2$ nanoplates were transformed into Co_3O_4 nanoplates without apparent change in morphology. In general, materials with hexagonal structure are favored to form 1-D nanostructures under a suitable reaction condition [24]. When the concentration of reactants increases, uniform nanowires are formed instead of nanoplates. However, a higher concentration of reactants (Fig. 2d, Sample 8) can cause the nanowires to become bigger or several single ones to merge. These phenomena might be caused by the rapid mass transfer and a large amount of high-energy sites on the surface of the as-prepared nanowires. When the concentration of reactants (Fig. 2c, Sample 7) was a little lower than the typical concentration (Sample 3), uniform and smooth nanowires were successfully obtained. However, the number density of the nanowires was sparser than the ones synthesized under the typical condition (Sample 3). The results suggest that the various morphologies of the

nanostructures can be tailored from nanoplates to nanowires by tuning the concentrations of $Co(NO_3)_2 \cdot 6H_2O$, and NH_4NO_3.

The effect of reaction temperature on the morphology of Co_3O_4 nanostructures is shown in Figure 3. In Fig. 3a (Sample 9), nanowires and several leaf-like crystals with diameters of 3–6 μm (measured in the middle of the leaf-like crystal) and lengths of approximately 16 μm were present. The surface of the leaf-like crystal was smooth and flat. Figure 3b (Sample 3) clearly shows that Co_3O_4 nanowires were uniformly covered with Ni foam, which grows densely and vertically from the substrate. The nanowires were uniform, with diameters of 500–900 nm and lengths of approximately 17 μm. In Fig. 3c (Sample 10), some of the nanowires grew bigger and longer, and a few of nanowires integrated into a bigger one. The coexistence of leaf-like crystals and nanowires suggests that the reaction process was not homogeneous when the temperature was 70º C. We do not understand the formation mechanism of the leaf-like crystal; however, we propose that this can be caused by the rapid gathering rate of local Co(II) ions. The reason for the enlargement of nanowires when the temperature was set at 100º C might be the rapid mass transfer, which led to a fast deposit of Co(II) ions on the nuclei. It could also be due to the increasing number of high-energy sites on the surface of nanowires, which led to the growth of nanocrystals among the as-prepared nanowires, thereby causing single nanowires to merge. The results suggest that temperature is a key factor in controlling the morphology of the nanowires. Well-ordered nanowire arrays were formed at the reaction temperature of 90º C.

To summarize the above discussions on the growth of Co_3O_4 nanowire arrays, various sizes of nanowires synthesized at different reaction conditions are shown in Table 1. The results suggest that the proper reaction condition for preparation of well-ordered nanowire arrays (Sample 3) were achieved as follows: a reaction time of 12 h, moderate concentration, and a temperature of 90º C. Figure 4 shows the XRD patterns of the samples prepared under this reaction condition. The phase of Ni was found in the pattern because of the Ni foam substrate. The XRD pattern of non-calcined nanowires contained the combined phases of brucite β-$Co(OH)_2$ and spinel Co_3O_4. Some Co(II) ions were oxidized to Co(III) ions during the nanowire growth in the solution. The pattern of Fig. 4b matches the pattern of spinel phase Co_3O_4 well, indicating that the nanowires were Co_3O_4 after calcination. The transformation of β-$Co(OH)_2$ to Co_3O_4 was due mainly to the oxidation of β-$Co(OH)_2$ during the calcination. The reaction formula was as follows:

$$6\ \beta\text{-}Co(OH)_2\ (s) + O_2\ (g) \rightarrow 2\ Co_3O_4\ (s) + 6\ H_2O\ (g) \qquad (1)$$

The TEM images (Fig. 5) show that the non-calcined nanowire was structural compact, while the calcined nanowire was loose and consisted of irregularly shaped cracks. Some cracks were formed from the release of water vapor during the calcination (refer to the reaction formula 1).

Figure 6a shows current-potential polarization curves of the Co_3O_4 nanowire and nanoparticle electrodes for electrochemical reduction of H_2O_2 in 0.4 M H_2O_2 and 3.0 M NaOH solution at scan rate 5 mV s^{-1}. The onset potentials of the two electrodes were quite similar at around -0.15 V. The catalytic activity of H_2O_2 electrochemical reduction is attributed to the redox couple of $Co(OH)_2/Co_3O_4$. The current density on the Co_3O_4

nanowire electrode was higher than that of the Co_3O_4 nanoparticle electrode in the tested potential range. More importantly, the Ni foam supported Co_3O_4 nanowire electrode showed a much lower potential at -0.6 V than that of the Co_3O_4 nanoparticle electrode (-0.35 V). The Co_3O_4 nanoparticle electrode delivered current density of 85.8 mA cm^{-2} at -0.35 V, which is comparable to literature [26]. In contrast, the Co_3O_4 nanowire electrode exhibited a higher current density of 101.8 mA cm^{-2} at -0.4 V compared to of the Co_3O_4 nanoparticle electrode. The high electrocatalytic performance of Co_3O_4 nanowires arises from the unique 1D nanostructures, which provide not only high surface area for electrochemical reaction but also a short diffusion path for ions. Such binder-free approach also results in low internal resistance because Co_3O_4 nanowires were in direct contact with the Ni foam substrate. Results clearly indicated that the Ni foam supported Co_3O_4 nanowire electrode exhibited superior catalytic activity and mass transport kinetics for H_2O_2 electrochemical reduction than binder approach powdery electrode. Figure 6b shows the dependence of the catalytic performance of Ni foam supported Co_3O_4 nanowire electrode (Sample 3) on various concentration of H_2O_2. The polarization curves demonstrated that H_2O_2 electrochemical reduction occurs at around -0.1 V and the current density increases with the potential going from -0.1 to -0.8 V. The cathodic peak current density increased with the increase of H_2O_2 concentration from 0.1 to 0.6 M. Significant small oxygen bubbles were observed on the electrode surface at an H_2O_2 concentration higher than 0.3 M. Currents began to fluctuate slightly when the potential was decreased from -0.45 to -0.8 V due to the perturbation of oxygen from H_2O_2 decomposition.

4. Conclusions

Various Co_3O_4 nanowires with different morphology and sizes grown on Ni foam were successfully prepared via a template-free method. The brucite β-$Co(OH)_2$ was transformed to spinel Co_3O_4 after calcination in air. The release of water vapor caused some cracks on the surface of the nanowires. Reaction temperature, the concentration of reactants, and reaction time are key variables that determine the final size and morphology of the nanowires. The nanowires grew vertically from the surface of the Ni foam, and both size and uniformity of the nanowires increased with the prolongation of reaction time. The nanowires synthesized at 12 h presented the most uniform morphology. The various morphologies of the nanostructures can be tailored from nanoplates to nanowires by tuning the concentration of reactants. The reaction temperatures lower or higher than 90º C were unfavorable to the growth of well-ordered nanowires. The Co_3O_4 nanowires were structurally uniform and crystalline and had diameters of approximately 500–900 nm and lengths of up to 17 μm in the typical reaction condition (Sample 3). The Ni foam supported Co_3O_4 nanowire electrode showed superior catalytic activity and mass transport property for H_2O_2 electrochemical reduction in an alkaline medium than the Co_3O_4 nanoparticle electrode.

Acknowledgements

This work was supported mainly by the Global Frontier R&D Program (2013M3A6B1078874) on Center for Hybrid Interface Materials (HIM) funded by the Ministry of Science, ICT & Future Planning, the Science and Technology Development Fund from Macau SAR (FDCT-098/2015/A3), and the UEA funding.

References

[1] D.J. Brodrecht, J.J. Rusek, Applied Energy, **74,** 113-124,
[2] X.H. Yan, T.S. Zhao, L. An, G. Zhao, L. Shi, Int J Hydrogen Energ, **41,** 5135-5140, (2016)
[3] S.M.M. Ehteshami, M. Asadnia, S.N. Tan, S.H. Chan, Journal of Power Sources, **301,** 392-395, (2016)
[4] S.J. Lao, H.Y. Qin, L.Q. Ye, B.H. Liu, Z.P. Li, Journal of Power Sources, **195,** 4135-4138, (2010)
[5] W.X. Yin, Z.P. Li, J.K. Zhu, H.Y. Qin, Journal of Power Sources, **182,** 520-523, (2008)
[6] D. Cao, L. Sun, G. Wang, Y. Lv, M. Zhang, Journal of Electroanalytical Chemistry, **621,** 31-37, (2008)
[7] F. Miomandre, P. Audebert, M. Maumy, L. Uhl, Journal of Electroanalytical Chemistry, **516,** 66-72, (2001)
[8] D. Cao, Y. Gao, G. Wang, R. Miao, Y. Liu, International Journal of Hydrogen Energy, **35,** 807-813, (2010)
[9] L. Sun, D. Cao, G. Wang, Journal of Applied Electrochemistry, **38,** 1415-1419, (2008)
[10] X.Z. Li, Y.Y. Fang, X.Q. Lin, M. Tian, X.C. An, Y. Fu, R. Li, J. Jin, J.T. Ma, J Mater Chem A, **3,** 17392-17402, (2015)
[11] A. Aijaz, J. Masa, C. Rosler, W. Xia, P. Weide, A.J.R. Botz, R.A. Fischer, W. Schuhmann, M. Muhler, Angew Chem Int Edit, **55,** 4087-4091, (2016)
[12] L. Xu, Q.Q. Jiang, Z.H. Xiao, X.Y. Li, J. Huo, S.Y. Wang, L.M. Dai, Angew Chem Int Edit, **55,** 5277-5281, (2016)
[13] T.T. Nguyen, V.H. Nguyen, R.K. Deivasigamani, D. Kharismadewi, Y. Iwai, J.J. Shim, Solid State Sci, **53,** 71-77, (2016)
[14] H.Y. Lu, Y.P. Huang, J.J. Yan, W. Fan, T.X. Liu, Rsc Adv, **5,** 94615-94622, (2015)
[15] S.X. Wu, K.S. Hui, K.N. Hui, K.H. Kim, J Mater Chem A, **4,** 9113-9123, (2016)
[16] L. Ren, K.S. Hui, K.N. Hui, J Mater Chem A, **1,** 5689-5694, (2013)
[17] L.J. Zhang, J. Wang, J.J. Zhu, X.G. Zhang, K.S. Hui, K.N. Hui, J Mater Chem A, **1,** 9046-9053, (2013)
[18] Y.-T. Tseng, J.-C. Lin, Y.-J. Ciou, Y.-R. Hwang, ACS Applied Materials & Interfaces, **6,** 11424-11438, (2014)
[19] S.X. Wu, K.S. Hui, K.N. Hui, J Phys Chem C, **119,** 23358-23365, (2015)
[20] Z. Guo, W. Liu, B.-L. Su, Nanotechnology, **19,** 1-5, (2008)
[21] G. Wang, D. Cao, C. Yin, Y. Gao, J. Yin, L. Cheng, Chemistry of Materials, DOI 10.1021/cm901928b(2009)
[22] Y. Shao, J. Sun, G. Lian, J Phys Chem C, **113,** 6566–6572, (2009)
[23] Y. Li, B. Tan, Y. Wu, Nanoletters, **8,** 265-270, (2008)
[24] Y. Hou, H. Kondoh, M. Shimojo, T. Kogure, T. Ohta, Journal of Physical Chemistry B, **109,** 19094-19098, (2005)
[25] X.W. Lou, D. Deng, J.Y. Lee, J. Feng, L.A. Archer, Advanced Materials, **20,** 258-262, (2008)
[26] D. Cao, J. Chao, L. Sun, G. Wang, Journal of Power Sources, **179,** 87-91, (2008)

1 Table 1. Various sizes of nanowires synthesized on different reaction conditions

Sample	Time (h)	Concentration (mol/l)			Temperature (℃)	Structure	Nanowire	
		Cobalt nitrate (mol/l)	Ammonium Nitrate (mol/l)	Ammonia (mol/l)			Diameter (nm)	Length (μm)
1	3	0.2	0.1	6	90	Wire	480~530	10~11
2	6	0.2	0.1	6	90	Wire	520~590	11~14
3	12	0.2	0.1	6	90	Wire	500~900	14~17
4	18	0.2	0.1	6	90	Wire	500~900	15~18
5	12	0.05	0.025	1.5	90	Plate		
6	12	0.1	0.05	3	90	Wire	300~400	2.5~3
7	12	0.15	0.75	4.5	90	Wire	400~550	9~11
8	12	0.25	0.125	7.5	90	Wire	Non-uniform	Non-uniform
9	12	0.2	0.1	6	70	Left like crystal + wire	NA	NA
10	12	0.2	0.1	6	100	Wire	800~6000	20~25

2

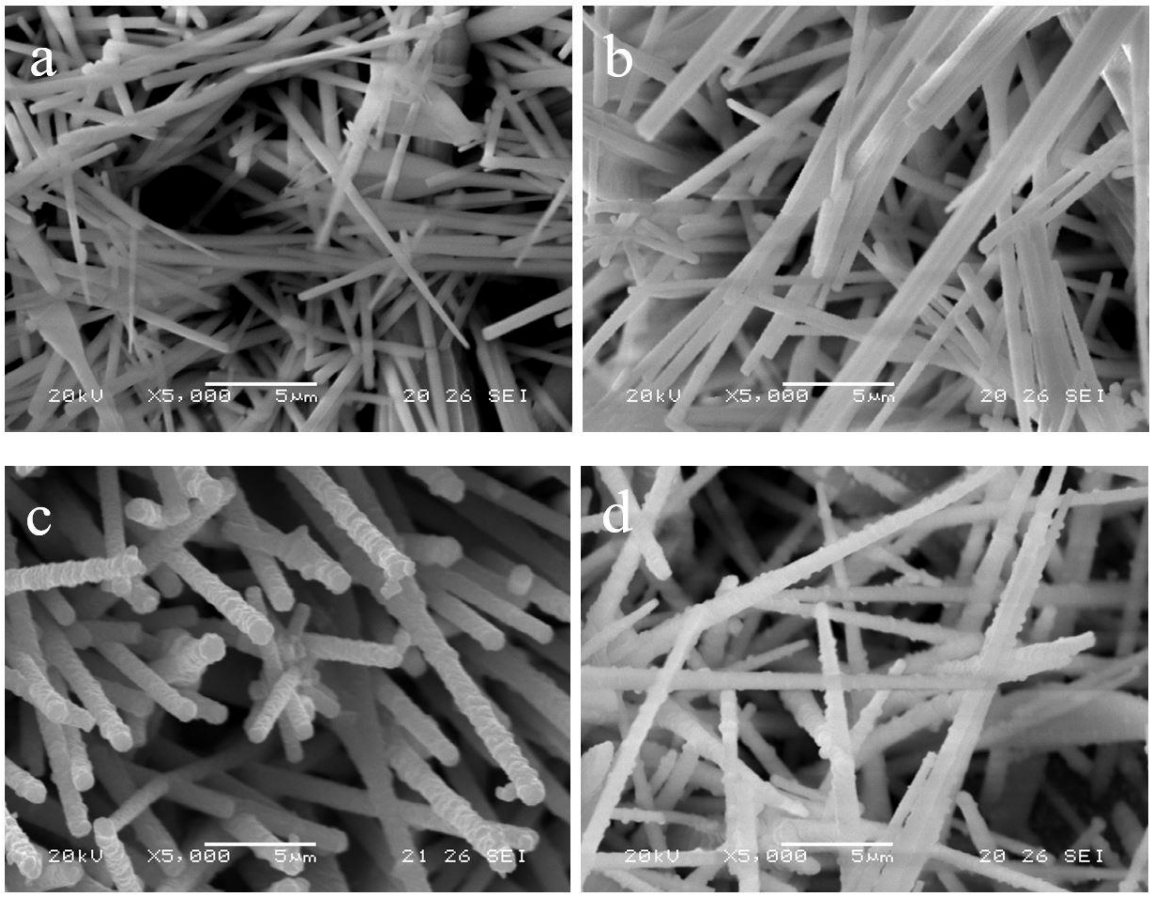

Fig. 1. SEM images of Co_3O_4 nanowire arrays grown at different times: **a** 3 h (Sample 1), **b** 6 h (Sample 2), **c** 12 h (Sample 3), **d** 18 h (Sample 4)

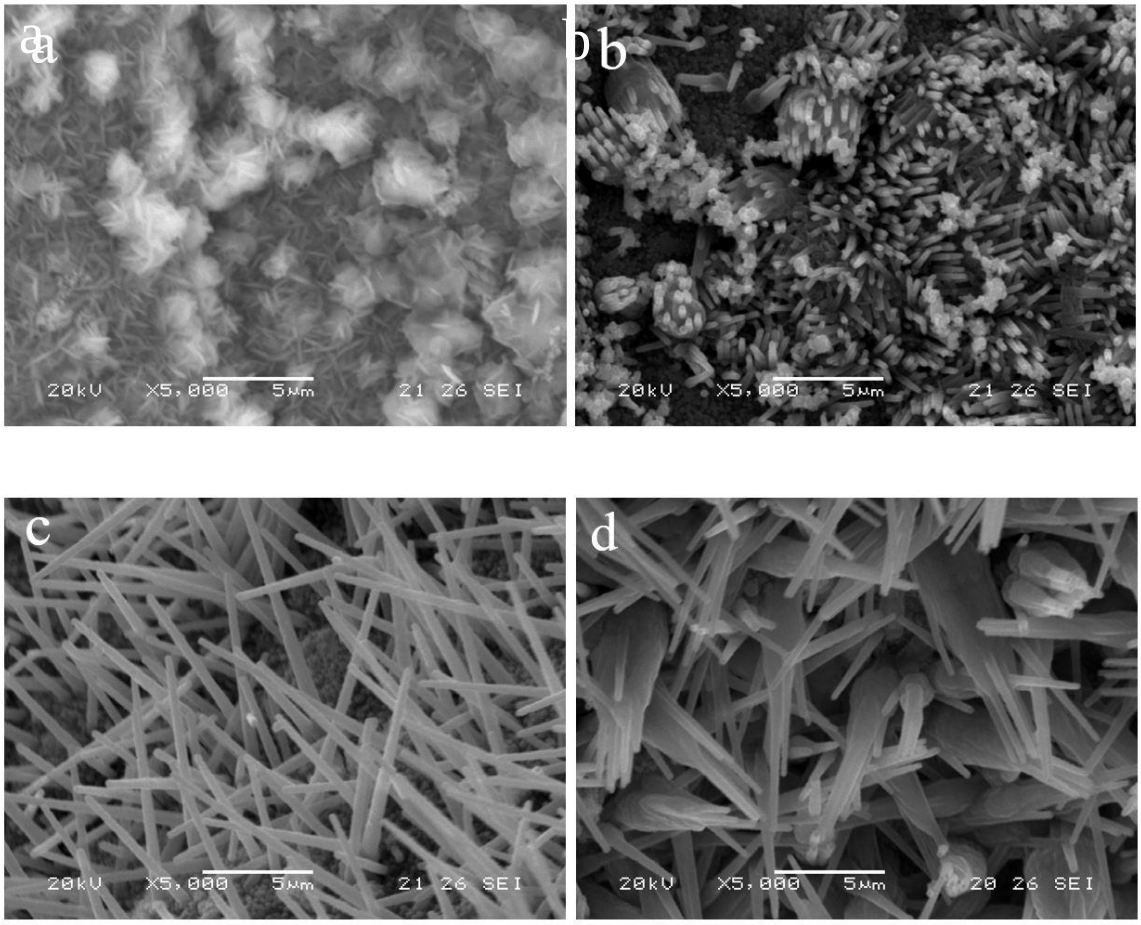

Fig. 2. SEM images of the nanoparticles or nanowires synthesized with different precursor concentrations: **a** Sample 5, **b** Sample 6, **c** Sample 7, **d** Sample 8

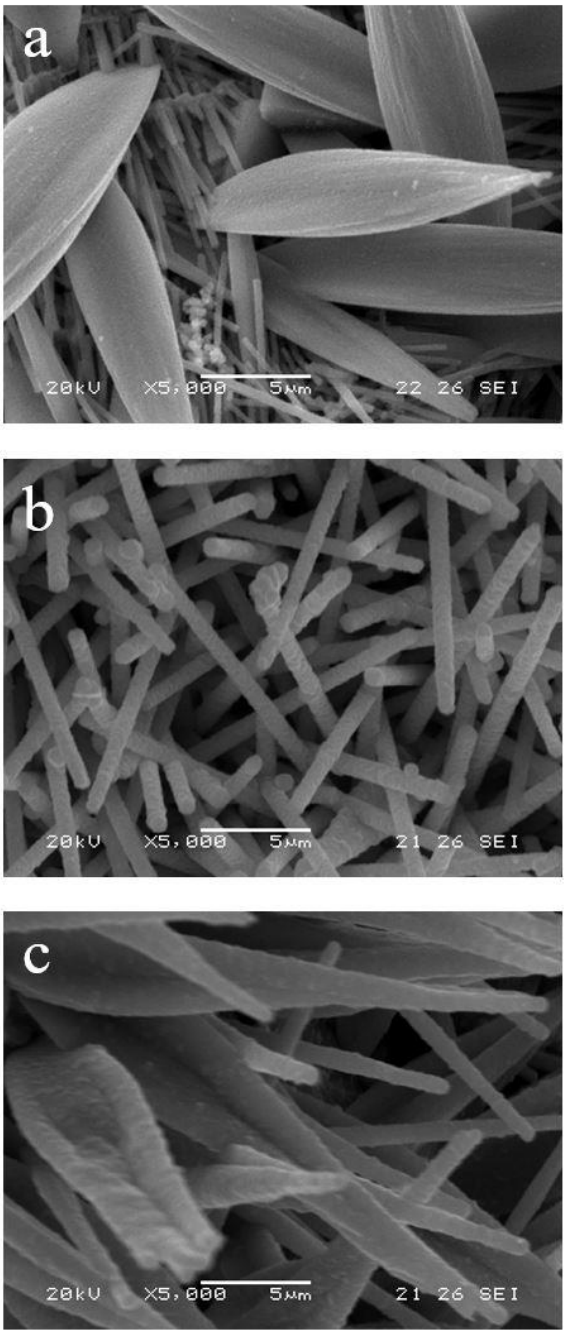

Fig. 3. SEM images of nanowires or other structures synthesized at different temperatures: **a** 70º C (Sample 9), **b** 90º C (Sample 3), **c** 100º C (Sample 10)

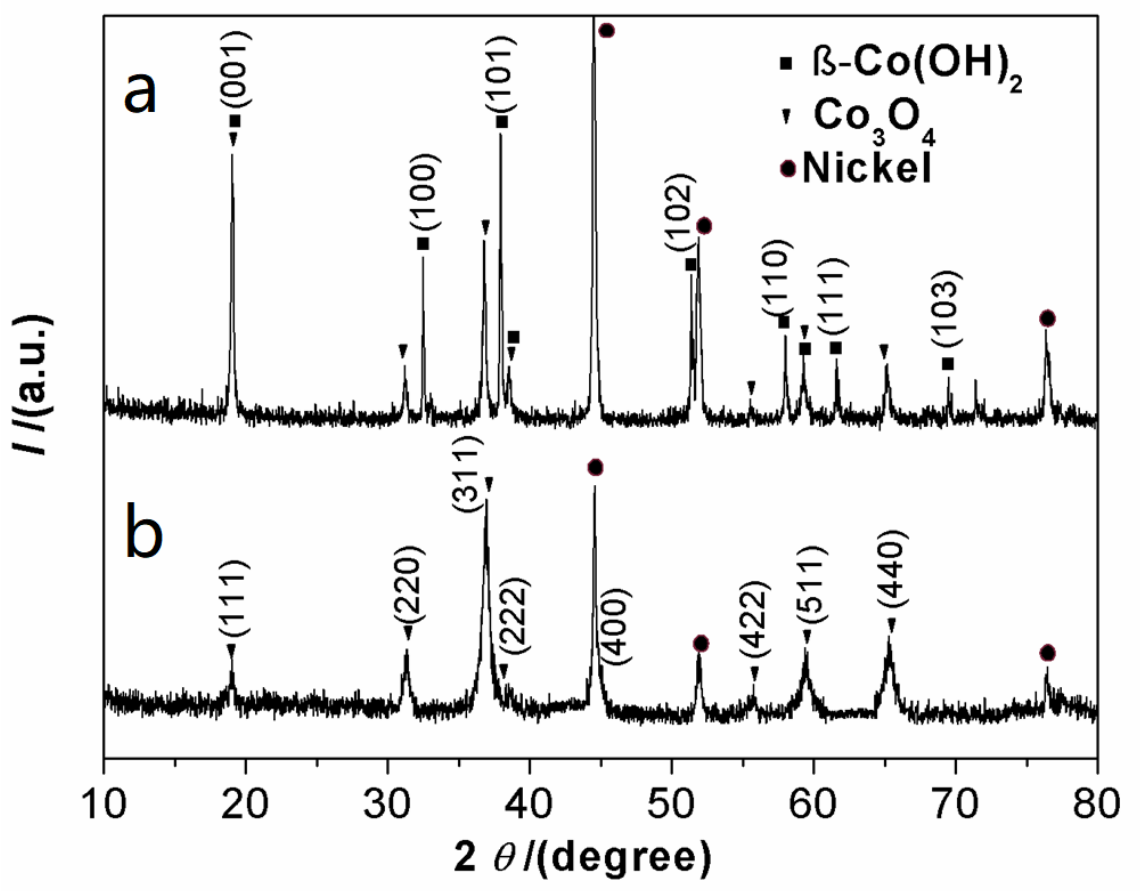

Fig. 4. XRD pattern of the nanowires scratched down from Ni foam substrate (Sample 3): **a** non-calcined, **b** calcined

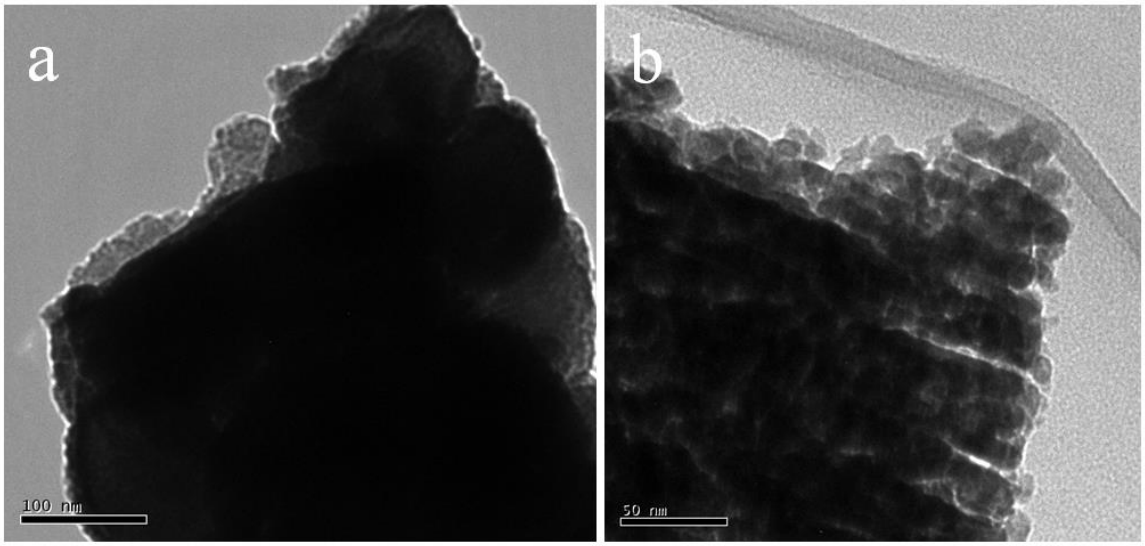

Fig. 5. TEM images of the nanowires (Sample 3): **a** non-calcined, **b** calcined

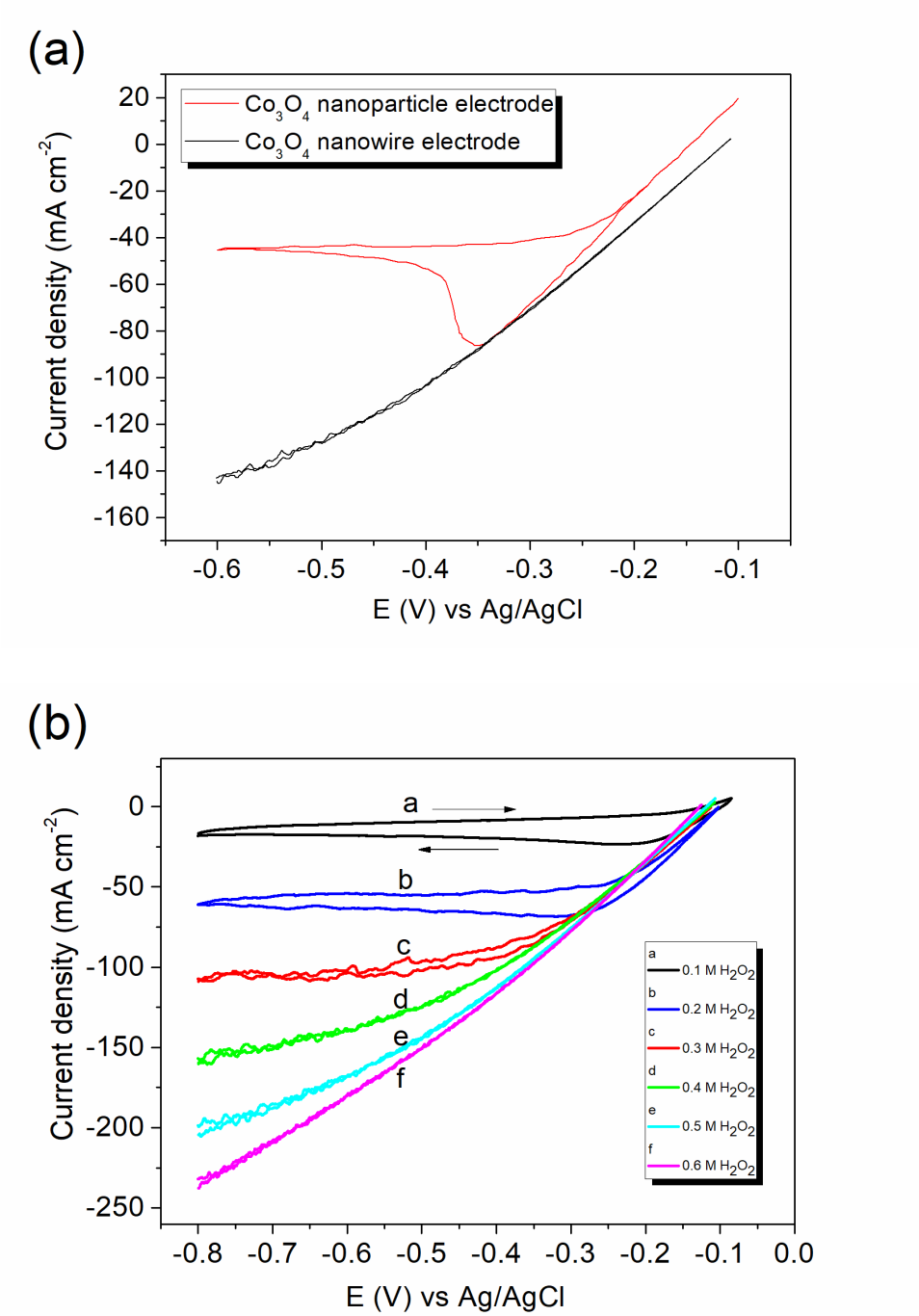

Fig. 6. Current-potential polarization curves for H_2O_2 electrochemical reduction: **a** Co_3O_4 nanoparticle and nanowire electrodes with electrolyte: 3.0 M NaOH and 0.4 M H_2O_2 at scan rate 5 mV s^{-1}, **b** Co_3O_4 nanowires electrode with electrolyte: 3.0 M NaOH and different concentrations of H_2O_2 at scan rate 5 mV s^{-1}.